Mon. Not. R. Astron. Soc. **000**, 1–11 (2007) Printed 1 February 2008 (MN LaTeX style file v2.2)

arXiv:0704.0586v1 [astro-ph] 4 Apr 2007

Dust Formation and Survival in Supernova Ejecta

Simone Bianchi[1] and Raffaella Schneider[2]
[1] *INAF - Istituto di Radioastronomia, Sezione di Firenze, Largo Enrico Fermi 5, 50125 Firenze, Italy*
[2] *INAF - Osservatorio Astrofisico di Arcetri, Largo Enrico Fermi 5, 50125 Firenze, Italy*

3 April 2007

ABSTRACT
The presence of dust at high redshift requires efficient condensation of grains in SN ejecta, in accordance with current theoretical models. Yet, observations of the few well studied SNe and SN remnants imply condensation efficiencies which are about two orders of magnitude smaller. Motivated by this tension, we have (i) revisited the model of Todini & Ferrara (2001) for dust formation in the ejecta of core collapse SNe and (ii) followed, for the first time, the evolution of newly condensed grains from the time of formation to their survival - through the passage of the reverse shock - in the SN remnant. We find that 0.1 - 0.6 $M_{\odot}$ of dust form in the ejecta of 12 - 40 $M_{\odot}$ stellar progenitors. Depending on the density of the surrounding ISM, between 2-20% of the initial dust mass survives the passage of the reverse shock, on time-scales of about $4-8\times10^{4}$ yr from the stellar explosion. Sputtering by the hot gas induces a shift of the dust size distribution towards smaller grains. The resulting dust extinction curve shows a good agreement with that derived by observations of a reddened QSO at $z = 6.2$. Stochastic heating of small grains leads to a wide distribution of dust temperatures. This supports the idea that large amounts ($\sim 0.1M_{\odot}$) of cold dust ($T \sim 40$K) can be present in SN remnants, without being in conflict with the observed IR emission.

Key words: dust, extinction - shock waves - supernova remnants - supernovae: individual (Cassiopeia A)

1 INTRODUCTION

In the last few years, mm and submm observations of samples of $5 < z < 6.4$ quasars have provided a powerful way of probing the very existence and properties of dust within 1 Gyr of the Big Bang. The inferred far-IR luminosities are consistent with thermal emission from warm dust ($T < 100$ K), with dust masses $\geqslant 10^{8} M_{\odot}$ (Bertoldi et al. 2003; Robson et al. 2004; Beelen et al. 2006; Hines et al. 2006). Despite the uncertainties due to the poorly constrained dust temperatures and absorption coefficients, the estimated dust masses are huge, implying a high abundance of heavy elements at $z \approx 6$, consistent with the super-solar metallicities inferred from the optical emission-line ratios for many of these systems (Pentericci et al. 2002; Freudling et al. 2003; Maiolino et al. 2003).

Although high redshift quasars are extreme and rare objects, hardly representative of the dominant star forming galaxies, the above observations show that early star formation leads to rapid enrichment of the Interstellar Medium (ISM) with metals and dust.

It is difficult for the dust to have originated from low-mass evolved stars at $z > 5$ as their evolutionary timescales (10^{8} to 10^{9} yr) are comparable to the age of the Universe at that time (Morgan & Edmunds 2003; Marchenko 2006). Thus, if the observed dust at $z > 5$ is the product of stellar processes, grain condensation in supernova (SN) ejecta provides the only viable explanation for its existence. This scenario has recently been tested through the observation of the reddened quasar SDSSJ1048+46 at $z = 6.2$ (Maiolino et al. 2004). The inferred extinction curve of the dust responsible for the reddening is different with respect to that observed at $z < 4$ (Small Magellanic Cloud-like, Hopkins et al. 2004), and it shows a very good agreement with the extinction curve predicted for dust formed in SN ejecta.

Theoretical models, based on classical nucleation theory, predict that a few hundred days after the explosions silicate and carbon grains can form in expanding SN ejecta, with condensation efficiencies in the range 0.1-0.3 (Kozasa et al. 1991; Todini & Ferrara 2001; Clayton et al. 2001).

Direct observational evidences for dust production have been collected only for a limited number of SNe, such as 1987A (Wooden et al. 1993) 1999em (Elmhamdi et al. 2003), and 2003gd (Sugerman et al. 2006). With the exception of 2003gd, the dust masses derived from the IR emission are $\approx 10^{-3} M_{\odot}$, corresponding to condensation efficiencies which are two orders of magnitude smaller than what theory predicts. A fraction of dust could escape detection if it is cold and concentrated in clumps. This has been confirmed to be the case for SN 2003gd where a radiative transfer code has been used to simultaneosly fit the optical extinction and IR emission, leading to an estimated dust mass of $2 \times 10^{-2} M_{\odot}$ (Sugerman et al. 2006). However, when applied to SN 1987A, the same numerical model gives dust mass estimates which do not differ significantly from previous analytic results (Ercolano et al. 2007).

Similar low dust masses have been inferred from infrared observations of galactic SN remnants with Spitzer and ISO satellites (Hines et al. 2004; Krause et al. 2004; Green et al. 2004). The consistent picture that emerges is that the mid- and far-IR excess observed is due to emission from small amounts of warm dust, with indicative temperatures $T \sim 80-270$ K and masses $3\times10^{-3}-10^{-5} M_{\odot}$ for Cas A, and temperatures $T \sim 50$ K and masses $3\times10^{-3}-0.02 M_{\odot}$ for the Crab nebula. Cold dust has also been detected through far-IR and submm observations of these remnants (Dunne et al. 2003; Krause et al. 2004). However, the interpretation of these data is complicated by the strong contamination from cold dust along the line of sight, providing so far only upper limits of $0.2 M_{\odot}$ on the amount of cold dust associated to the SN remnants.

The aim of the present paper is to critically assess the model developed by Todini & Ferrara (2001) exploring a wider range of initial conditions and model assumptions. We then follow the evolution of dust condensed in SN ejecta on longer timescales with respect to previous theoretical models. In particular, we are interested in understanding how the passage of the reverse shock affects the newly formed grain size distributions and masses, so as to make predictions for the expected dust properties from the time of formation in the ejecta (a few hundred days after the explosion) to its survival in the SN remnant, hundreds of years later. So far this process has received little attention, most of the studies being dedicated to the destruction of ISM dust grains caused by the SN forward shock (Draine & Salpeter 1979; Jones et al. 1994; Nozawa et al. 2006), with the notable exception of Dwek (2005), who, on the basis of timescale considerations, finds that the reverse shock is able to destroy much of the initially formed dust.

The paper is organised as follows: Sect. 2 revisits the dust formation models based on the nucleation theory; Sect. 3 describes the model adopted for the propagation of the reverse shock into the ejecta and shows the effect of sputtering on the grain size distribution and total mass; in Sect. 4 we compare the extinction and emission properties of the surviving SN dust with observations. Finally, the results are summarised in Sect. 5.

2 SN DUST FORMATION REVISITED

Models of dust formation in the ejecta of core collapse SNe typically predict that large masses of dust ($0.1-1.0 M_{\odot}$) are formed within 1000 days from the onset of the explosion, when the ejecta are still compact (radius of order 10^{16}cm; Kozasa et al. 1991; Todini & Ferrara 2001; Nozawa et al. 2003). If these freshly formed dust grains were distributed homogeneously within the ejecta, their opacity would be very high, with center-to-edge optical depths of order 10^2-10^4 in optical wavelengths, depending on the grain material and size distribution. The ejecta would thus be opaque to radiation produced within it (Kozasa et al. 1991).

Observations of recent SNe, instead, reveal extinctions smaller than a couple of magnitudes, which imply dust masses of only $10^{-4}-10^{-2} M_{\odot}$ (Sugerman et al. 2006; Ercolano et al. 2007). The dust mass derived from extinction measures could be underestimated if grains are distributed in clumps with a small volume filling factor: for a given amount of grains, a clumpy distribution would produce a lower effective extinction. However, the comparison between observations of dust extinction/emission and radiative transfer models shows that the neglect of clumping can only produce a moderate underestimation of the dust mass in the ejecta (Ercolano et al. 2007).

To check whether the dust production in SNe is overestimated, we have reconsidered the model of Todini & Ferrara (2001). In the model, dust formation is investigated in the framework of standard nucleation theory: when a gas becomes supersaturated, particles (monomers) aggregate in a seed cluster which subsequently grows by accretion of other monomers (Feder et al. 1966). For grain materials whose molecules are not present in the gas phase, the *key species* approach is adopted (Kozasa & Hasegawa 1987). Six materials where considered in the original work: amorphous carbon (AC), iron, corundum (Al_2O_3), magnetite (Fe_3O_4), enstatite ($MgSiO_3$) and forsterite (Mg_2SiO_4). Following Schneider et al. (2004), we have added the formation of SiO_2 grains. SiC grains, found in meteorites and considered to be of SN origin from their anomalous isotopic ratios (Clayton & Nittler 2004), are not considered since their formation is impeded by the formation of AC and Si-bearing grains (Nozawa et al. 2003). The model of Todini & Ferrara also considers the formation and destruction of SiO and CO molecules: while the first is necessary to study the formation of Si-bearing grains, the second may be a sink for carbon atoms that otherwise would accrete on grains.

The ejecta are taken to have a uniform composition and density, with initial temperature and density chosen to match the observations of SN1987A. The initial composition depends on the metallicity and mass of the progenitor star, $M_{\rm star}$, while the dynamic is given by the mass of the ejecta $M_{\rm eje}$ and the kinetic energy of the explosion $E_{\rm kin}$: the models of Woosley & Weaver (1995) were used.

In the models of Todini & Ferrara, the gas becomes supersaturated after a few hundred days from the explosion. The nucleation process starts at temperature between 1800K (for AC) and 1200K (for Si-bearing materials). At the beginning the gas is moderately supersaturated and large seed clusters, made of $\mathcal{N}$ monomers, tend to form. However, their formation rate per unit volume (*the nucleation current*) is small. As the volume of the ejecta increases, the supersaturation rate grows and smaller clusters aggregate with a larger formation rate. This occurs until the gas becomes sufficiently rarified (because of expansion and/or exhaustion of monomers in the gas phase) and the formation rate drops. The nucleation process, together with accretion, results in a typical log-normal grain size distributions (see, e.g., Todini & Ferrara 2001; Nozawa et al. 2003).

For materials apart from AC, the supersaturation rate increases quickly during the ejecta expansion, and the seed clusters can become very small. In Todini & Ferrara (2001) seed clusters were allowed to be of any size. In this paper we

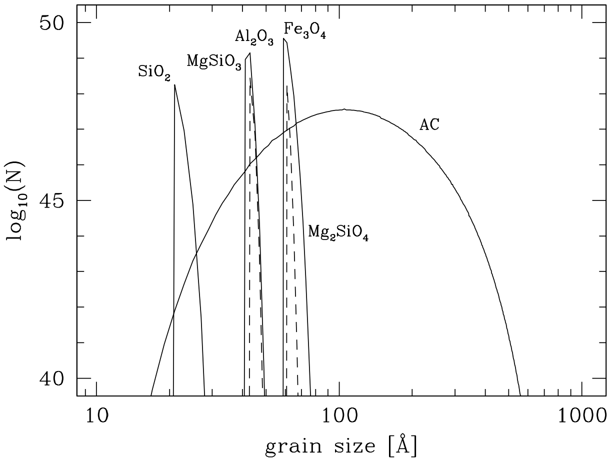

Figure 1. Size distribution for grains formed in the ejecta of a SN with a progenitor star of solar metallicity and mass $M_{\rm star} = 20 M_\odot$ ($\mathcal{N} = 2$). The distributions of Al_2O_3 and Mg_2SiO_4 are shown with dashed lines for ease of identification.

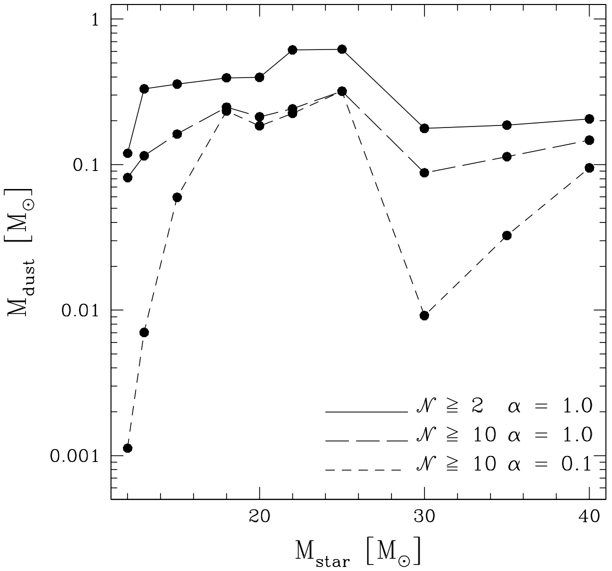

Figure 2. Mass of dust formed in the ejecta of a SN as a function of the mass of the progenitor star, for models with different minimum cluster size and sticking coefficient. The metallicity of the progenitors is solar.

consider only clusters with $\mathcal{N} \geqslant 2$, and introduce discrete accretion of monomers. While these two (more physical) requirements have a limited effect on AC grains, they alter the size distributions and masses of grains composed by the other materials. In Fig. 1 we show the size distribution of grains formed in the ejecta of a SN with a progenitor star of solar metallicity and $M_{\rm star} = 20 M_\odot$. Only AC grains retain the usual log-normal distribution. Instead, the size distribution of grains of other materials lacks the low-radius tail. Compared to the results of Todini & Ferrara (2001), their total number is reduced (since larger seed clusters have a smaller formation rate) and their mean size is larger (since the monomers not allowed to form the smaller clusters are now available to accrete on the larger).

It is to be noted, however, that the use of the standard nucleation theory is questionable when clusters are made by $\mathcal{N} \lesssim 10$ monomers (Draine 1979; Gail et al. 1984). To check what influence this limit has on the results, we have run models in which the formation of clusters with $\mathcal{N} < 10$ is suppressed. The resulting size distributions confirm the same trend: less non-AC grains form, and of larger mean size. Again AC is unaffected.

In Fig. 2 we show $M_{\rm dust}$, the mass of dust formed in the ejecta of SNe of solar metallicity, as a function of $M_{\rm star}$. The solid line refer to the models with $\mathcal{N} \geqslant 2$. Though reduced with respect to Todini & Ferrara, still considerable masses of dust are formed, predominantly of AC and Fe_3O_4 grains. If $M_{\rm star} \leqslant 25 M_\odot$, all the available carbon condenses in dust grains. In the more massive models, roughly equal amounts of carbon goes in grains and in CO, since the molecule destruction mechanism provided by ^{56}Co decay is reduced because of its low yield in the ejecta. Results are similar (within a factor of two) if the metallicity of the progenitor stars is below solar. The only distinction is the model with zero metallicity, where stars with $M_{\rm star} \geqslant 35 M_\odot$ produce no dust (Schneider et al. 2004). No substantial differences are found if a different thermal history of the ejecta is assumed: M_{dust} is still of the same order of magnitude if densities and temperatures follow the evolution adopted by Nozawa et al. (2003). As already seen in Fig. 1, imposing $\mathcal{N} \geqslant 10$ results in a great reduction of the number of non-AC grains: the dust mass in these models is entirely due to AC, which is unaffected by the limit (Fig. 2, long-dashed line).

Dust formation models depend strongly on the sticking coefficient α. In most of the published models, and in the results presented so far, it is assumed that all gas particles colliding on a grain will stick to it ($\alpha = 1$). However, theory predicts that α depends on the impact energy, on the grain internal energy, and on the material involved: for the gas temperature at which most grains form α is significantly reduced (Leitch-Devlin & Williams 1985). Indeed, laboratory experiments on the formation of cosmic dust analogs shows that $\alpha \approx 0.1$ for Si-bearing grains (Gail 2003). Thus, we have also run models assuming $\alpha = 0.1$ for all the species considered. By reducing α, monomers stay in the gas phase longer and dust formation is delayed to times when supersaturation is larger: typically, smaller seed clusters form. For $\mathcal{N} \geqslant 2$, the number of non-AC grains is further reduced and their mass becomes negligible compared to that of AC. Again all available carbon is locked in AC grains, but their size distribution is shifted towards lower radii and seed clusters form with $\mathcal{N} < 10$. For $\mathcal{N} \geqslant 10$ (Fig. 2, dashed line) their mass reduces and the size distribution becomes similar to those of non-AC grains in Fig. 1. At least for low mass progenitors, the predicted M_{dust} are closer to the values inferred by observations.

Clearly, the thermodynamic properties of the ejecta are at the limits of applicability of classical nucleation theory. A different approach may be needed, expecially if realistic α values are taken into account. Unless otherwise stated, in the following we will study the evolution of dust grains resulting from models with solar metallicity for the SN progenitors and $\mathcal{N} \geqslant 2$, $\alpha = 1$ (so as to conform to most works in literature). However, we will also discuss the results for models with different assuptions on $\mathcal{N}$ and α.

3 SURVIVAL IN THE REVERSE SHOCK

As the ejecta expands, a forward shock is driven into the ISM, which compresses and heats the ambient gas. The ISM becomes an hostile environment for the survival of dust grains preexisting the SN event, mainly because of sputtering by collisions with gas particles (Draine & Salpeter 1979; Jones et al. 1994; Nozawa et al. 2006). In turn, the shocked ambient gas drives a reverse shock in the ejecta, which, by about 1000 years, has swept over a considerable fraction of its volume. The dust within the SNe, then, has to face hostile conditions inside what had previously been its cradle. We study the process in this Section.

3.1 Dynamics of the reverse shock

Truelove & McKee (1999) have studied the dynamics of a SN remnant through its nonradiative stages, the ejecta dominated and the Sedov-Taylor. They provide analytic approximations for velocity and position of the reverse and forward shocks, as a function of the kinetic energy $E_{\rm kin}$ and mass $M_{\rm eje}$ of the ejecta, and of the ISM density $\rho_{\rm ISM}$. We use here their solution for a uniform density distribution inside the ejecta. The values for $E_{\rm kin}$ and $M_{\rm eje}$ are the same that were used in the dust formation models: $E_{\rm kin} = 1.2 \times 10^{51}$ erg and $10 M_\odot \lesssim M_{\rm eje} \lesssim 30 M_\odot$ for stellar progenitor masses in the range 12-40 $M_\odot$ and metallicities between zero and solar (Woosley & Weaver 1995). We study the effect of three different ISM environments, with $\rho_{\rm ISM} = 10^{-25}$, 10^{-24} and 10^{-23} g cm^{-3}.

For each model, we have divided the ejecta into $N_{\rm s}$ spherical shells. We have assumed that all shells have the same initial width $\Delta R = R_{\rm eje}/N_{\rm s}$, with $R_{\rm eje}$ the initial radius of the ejecta. The mass of each shell is conserved throughout the evolution. For the j shell (counting shells outwards), the initial velocity of the gas at its inner boundary is given by homologous expansion,

$$v_j = v_{\rm eje} \frac{R_j}{R_{\rm eje}}, \qquad v_{\rm eje} = \sqrt{\frac{10}{3} \frac{E_{\rm kin}}{M_{\rm eje}}}, \tag{1}$$

where R_j is the initial radius of the inner shell boundary and $v_{\rm eje}$ is the velocity of the external boundary for ejecta of uniform density. For practical purposes, we start our simulation at a time t_0 (ideally, $t_0 \to 0$), and we set $R_{\rm eje} = v_{\rm eje} t_0$. The results do not depend on the exact value of t_0, provided it is taken small enough (we use a value of order a few tens of years).

After setting the initial conditions, we study the evolution of the ejecta with time. At each time step, the reverse shock goes inward through a single shell. Thus, at time t_i, the reverse shock has travelled inward through i shells, and lies at the inner boundary of shell $j_{\rm rs} = N_{\rm s} - i - 1$. Shells that have not been visited by the reverse shock (for $0 \leqslant j \leqslant j_{\rm rs} - 1$) continue to follow homologous expansion, i.e. the inner and outer radii grow linearly with time, with velocity given by Eq. 1. Following the shell expansion (increase in the shell volume V_j), the shell gas density decreases as $\rho_j \propto V_j^{-1}$. For an adiabatic expansion, the shell temperature scales as $T_j \propto V_j^{1-\gamma}$, with $\gamma = 5/3$ (Truelove & McKee 1999). Since the shock is strong, the results are independent on the initial choice for the gas temperature in the ejecta.

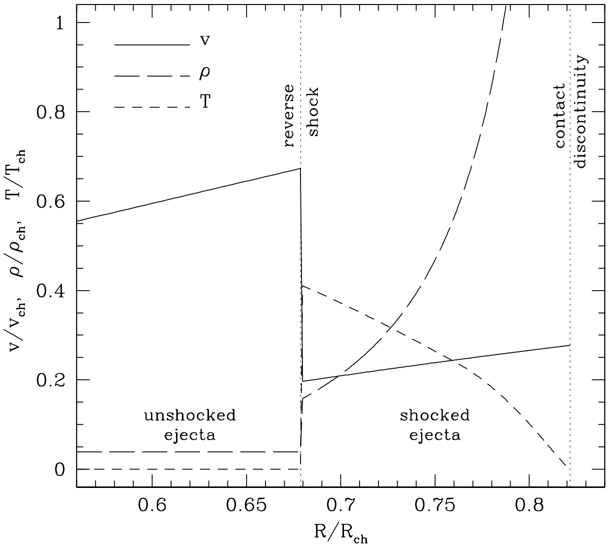

Figure 3. Velocity, density and temperature of the ejecta at $t = t_{\rm ch}$ as a function of the radius, for the model with progenitor star of solar metallicity and mass $M_{\rm star} = 20 M_\odot$ ($M_{\rm eje} = 18 M_\odot$) expanding in a ISM with density $\rho_{\rm ISM} = 10^{-24}$ g cm^{-3}. All quantities are normalised to their *characteristic* values (Truelove & McKee 1999). For the model shown here $t_{\rm ch} = 5800$ yr, $R_{\rm ch} = 10.7$ pc, $T_{\rm ch} = 5.7 \times 10^7$ K, $v_{\rm ch} = 1800$ km s^{-1}. It is also $\rho_{\rm ch} = \rho_{\rm ISM}$. The *contact discontinuity* marks the border between the shocked ejecta and the ISM swept by the forward shock.

For the shell $j = j_{\rm rs}$ that has been swept over by the shock at time t_i, we apply the standard Rankine-Hugoniot jump conditions for a strong adiabatic shock. The density, velocity and temperature change as

$$\rho_j = \frac{\gamma+1}{\gamma-1} \rho'_j,$$

$$v_j = v'_j - \frac{2}{\gamma+1} \tilde{v}_{\rm rs},$$

$$T_j = 2 \frac{\gamma-1}{(\gamma+1)^2} \frac{m}{k} \tilde{v}_{\rm rs}^2,$$

where ρ'_j and v'_j are the density and velocity before the shock (i.e. following the same evolution as for shells with $j < j_{\rm rs}$), $\tilde{v}_{\rm rs}$ is the velocity of the reverse shock in the reference frame of the unshocked ejecta (provided by Truelove & McKee 1999), m is the mean particle mass and k the Boltzmann's constant. To ensure mass conservation, the volume of shell $j = j_{\rm rs}$ is reduced by a factor $(\gamma-1)/(\gamma+1)$.

For the shells $j_{\rm rs} < j < N_{\rm rs}$ shocked at earlier times $t < t_i$, we compute the velocity v_j by interpolating between the velocity of the $j = j_{\rm rs}$ shell and the velocity of the forward shock (in the ambient rest frame), as a function of the logarithm of the shell inner radius. Velocity and position of the forward shock are also given by Truelove & McKee (1999). As for shells with $j < j_{\rm rs}$, the evolution of density and temperature is derived from the condition of adiabatic expansion and conservation of the shell mass. The typical trends for velocity, density and temperature around the reverse shock are shown in Fig. 3.

We checked the results (in particular the assumption for the evolution of $j > j_{\rm rs}$ shells) with the 1-D hydrodynamical models of SN blast waves of van der Swaluw et al. (2001) and with simulations kindly provided by L. Del Zanna (based on the code described in Del Zanna et al. 2003). However crude, our approximation provide a simple and fast solution for the density and temperature evolution of the ejecta during the passage of the reverse shock. Chosing an adequate number of shells (we use $N_{\rm s} = 400$), it agrees with the complete hydrodynamical solution within a factor of 2.

3.2 Dust grain survival

We assume that dust grains are distributed uniformly within the ejecta, and that the size distribution is the same everywhere. In the shells that have been visited by the reverse shock, dust grains are bathed in a gas heated to high temperature (of order $10^7 - 10^8$ K for the cases studied here). Also, the gas is slowed down and dust grains decouple from it, attaining a velocity relative to the gas

$$v_{{\rm d}j} = \frac{2}{\gamma+1}\tilde{v}_{\rm rs}.$$

Gas particles thus impact on dust grains transferring thermal and kinetic energy, which are of the same order of magnitude (both depending on the reverse shock velocity $\tilde{v}_{\rm rs}$, which is of order 10^3 km s^{-1}). Thermal and non-thermal sputtering result, which erode the dust grain, reducing its size. Eventually, the gas drag due to direct and Coulomb collisions slows the grain and non-thermal sputtering weakens. In this work we consider both thermal and non-thermal sputtering, but we neglect the gas drag and the grain charge: once passed through the reverse shock, the grain retains its velocity relative to the gas. We can thus provide upper limits on the influence of non-thermal sputtering.

The number of atoms that are sputtered off a dust grain per unit time is given by the sputtering rate dN/dt, a complex function of the gas density, temperature and of the nature of the dust/gas (target/projectiles) interaction (full expressions for dN/dt can be found elsewere, see e.g. Bianchi & Ferrara 2005). The sputtering rate depends on the sputtering yield, Y, the fraction of atoms that leave the target per projectile collision, which is a function of the energy of the impact. We use here the Y functions described in Nozawa et al. (2006), and we consider collisions of dust grains with H, He and O atoms in the ejecta. The grain radius decreases with sputtering as

$$\frac{da}{dt} = -\frac{a_{\rm m}^3}{3qa^2}\frac{dN}{dt}, \qquad (2)$$

where, q is the number of atoms in a molecule of the grain material, and $a_{\rm m}$ is the *molecule radius*, computed from the material density and the molecule mass. The values for $a_{\rm m}$ can be derived easily from the a_{0j} values of Table 2 in Nozawa et al. (2003). At each time step, we reduce the grain size according to Eq. 2 in all shells that have been swept by the reverse shock. We follow the evolution until the reverse shock arrives near the center of the ejecta: this is the limit of validity of the approximations in Truelove & McKee (1999). After that, we simply assume that the ejecta expands adiabatically, and we end the simulations when the sputtering rate becomes negligible. Since we do not include gas drag and grain charge, grains do not attain differential velocities for different sizes. Thus, we have neglected destruction due to grain-grain collisions. However, sputtering dominates over this process for the high shock velocities considered here (Jones et al. 1994).

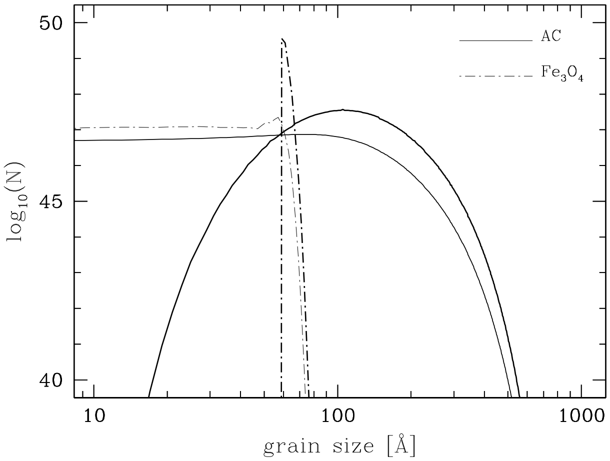

Figure 4. Changes in the size distribution of AC and $\rm Fe_3O_4$ grains. For each material, the thick line is the initial size distribution (the same as in Fig. 1). The thin line is the size distribution after the passage of the reverse shock through the ejecta.

Dust grains in the ionized shocked gas are heated mainly by collisions with electrons. If the grains are small, heating is stochastic and an equilibrium temperature does not exist. Instead, a broad temperature distribution $P(T_{\rm d})$ establishes, peaking at low temperature but extending also to high values (Dwek 1986). The temperature may be so high that dust grains sublimate (Guhathakurta & Draine 1989). For the cases studied here, however, sublimation is negligible. Details on the calculation are presented in Appendix A.

In Fig. 4 we show the initial (thick lines) and final (thin lines) size distributions for AC and $\rm Fe_3O_4$ grains in the ejecta of a star with $M_{\rm star} = 20 M_\odot$ expanding in a medium with $\rho_{\rm ISM} = 10^{-24}$ g cm^{-3}. As it is evident for the (initially) more peaked size distributions of magnetite, sputtering produces a *leaking* towards smaller sizes. The evolution of the size distribution is analogous to that of ISM grains destroyed by the forward shock (Nozawa et al. 2006).

In Fig. 5 we show the mass of dust that survives the passage of the reverse shock. For the reference model (dashed line), the erosion caused by sputtering reduces the dust mass to about 7% of its initial value, almost independently of the stellar progenitor model. Most of the dust (about 70% in mass) is consumed within one *characteristic time* $t_{\rm ch}$ from the explosion, when 95% of the original volume of the ejecta has been reached by the reverse shock ($t_{\rm ch} = 4{-}8\times10^4$ yr for the ejecta discussed here; Truelove & McKee 1999). Dust in the inner shells is less affected by erosion, because the sputtering rate is lower. A minor fraction of the dust mass, less than 10%, is consumed after the reverse shock bounces at the center of the ejecta (for $t \gtrsim 2.6 t_{\rm ch}$; Truelove & McKee 1999).

If the SN explodes in a denser ISM, the reverse shock would travel faster inside the ejecta and would encounter a gas at higher density. This increases the effect of sputtering. In Fig. 5 (long-dashed line) we see the fraction of dust mass that survives when $\rho_{\rm ISM} = 10^{-23}$ g cm^{-3}: only about 2% of the dust mass survives. Conversely, for a lower density ISM, a larger fraction is left: for $\rho_{\rm ISM} = 10^{-25}$ g cm^{-3}, it is 20%

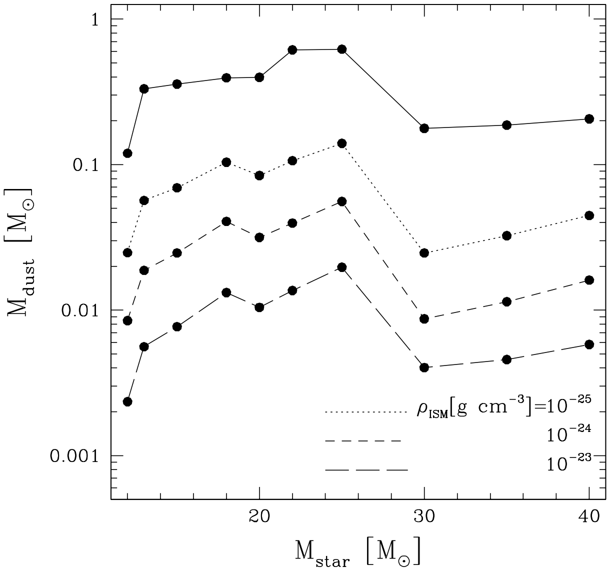

Figure 5. Mass of dust that survives the passage of the reverse shock in the ejecta, as a function of the mass of the progenitor star and of the density of the surrounding ISM. The solid line shows the initial dust mass (same as the solid line in Fig. 2).

(dotted line). While the number of surviving grains changes with the ISM density, the shape of the size distributions remain similar in all cases, with the typical patterns shown in Fig. 4.

No substancial change is observed in models where the dust was produced by progenitors of metallicity different from solar. Dust destruction is instead enhanced in models where a smaller sticking coefficient is adopted. If $\alpha = 0.1$ (Sect. 2), only 10, 3 and 1% of the original dust mass survives, respectively, for $\rho_{\rm ISM} = 10^{-25}$, 10^{-24} and 10^{-23} g cm^{-3} (compared to 20, 7 and 2% for $\alpha = 1.0$). This is because for smaller values of α, the dust distribution is made by grains of smaller radii, which are more easily destroyed.

4 EXTINCTION AND EMISSION FROM SN DUST

Maiolino et al. (2004) measured the reddening in the rest-frame UV spectrum of a $z = 6.2$ QSO and found it to be different from that of the SMC, typically used to deredden the spectra of lower redshift QSOs. The measured reddening is instead compatible with the extinction law from the Todini & Ferrara (2001) SN dust model. We repeat here the same analysis using the updated dust formation models of Sect. 2 and the final distributions after the reverse shock passage of Sect. 3. As in Maiolino et al. (2004), we derive the extinction properties from the grain sizes using the Mie's (1908) theory for spherical dust grains and refractive indexes for dust materials from the literature (references are provided in Table A1). The procedure is analogous to that adopted by Hirashita et al. (2005) when modelling the dust extinction from the SNe dust models of Nozawa et al. (2003).

In Fig. 6 we show the results for dust formed in SNe from progenitors of solar metallicity. The grain size distributions from progenitors of different masses have been averaged over a stellar Initial Mass Function (IMF): we adopted the Salpeter IMF, but the results do not depend heavily on this choice (Maiolino et al. 2004). The thick solid line represents the extinction law of dust as formed within the ejecta, without taking into account the grain processing caused by the reverse shock. The SN dust extinction law is still flatter than the SMC extinction law, but the agreement with the observations (shaded area) is worse than in Maiolino et al. (2004). This is mainly due to a change in the grain materials that contribute to extinction: apart from AC, present in both the old and new model, the rise at $\lambda < 2000$ Å was due to Mg_2SiO_4 grains, with a minor contribution from Fe_3O_4. In the new model, Mg_2SiO_4 contribution is insignificant, while Fe_3O_4 grains (larger than in the original model) cause the far UV rise. The bump at $\lambda \approx 2500$ Å is due to AC grains and it is typical of the optical properties derived from amorphous carbon formed in an inert athmosphere (the *ACAR* sample of Zubko et al. (1996)).

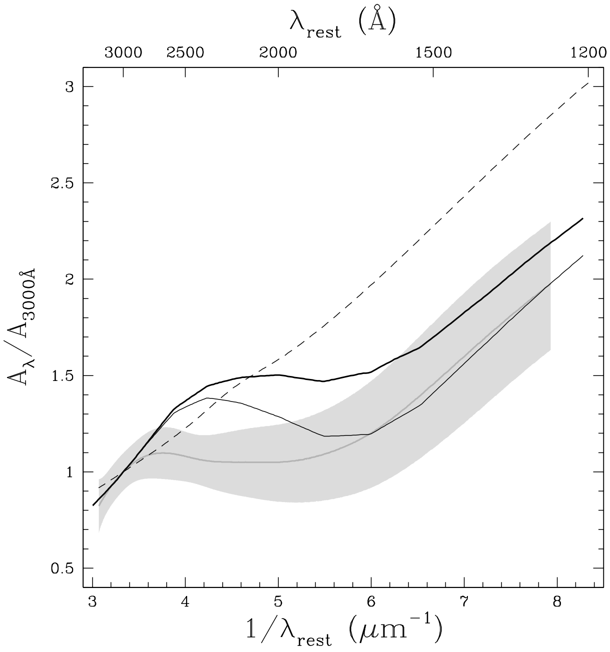

Figure 6. Extinction law for SN dust. The thick solid line is the extinction law for dust freshly formed in the ejecta. The thin solid line is the extinction law from dust processed by the reverse shock. The curves are computed from the IMF-averaged size distributions of grains formed in SNe from solar metallicity progenitors (see text for details). The gray line and shaded area are the extinction law measured on a $z = 6.2$ QSO and its uncertainty (Maiolino et al. 2004). The dashed line is the extinction law of the SMC (Pei 1992).

During the passage of the reverse shock, Fe_3O_4 grains are consumed more effectively than AC grains. The resulting extinction law (thin solid line in Fig. 6) becomes flatter, leading to an excellent agreement with observations at $\lambda \leqslant 1600$ Å. These results apply for ejecta expanding in a medium with $\rho_{\rm ISM} = 10^{-24}$ g cm^{-3}. There is no significant change in the extinction law if different ISM densities are considered, since the size distributions are similar in all cases (though the extinction at any given wavelength is smaller for higher $\rho_{\rm ISM}$, because less grains survive). It is worth noting that grains with $a \lesssim 20$ Å though as abundant as larger grains, do not contribute to the extinction law because of their reduced extinction cross section. As in Maiolino et al. (2004), we find that if progenitors of metallicity lower than solar are considered, the difference in the resulting extinction laws are small and lie within 0.1 y-axis units from the lines plotted in Fig. 6.

Extending calculations to the infrared, we have derived the dust emissivity. For all the IMF averaged size distributions, the emissivity in the wavelength range $10 \leqslant \lambda/\mu m \leqslant 1000$ is rather featureless, and can be well described by a power law in wavelength of index -1.4 with $\kappa(100\mu m) = 40$ cm^2 g^{-1} for models where all dust has been processed by the reverse shock. Emissivities for dust formed from progenitors of a given mass are within 10% of the IMF averaged value, while the emissivity at the end of dust condensation, before any significant sputtering has occurred, is found to be about 20% lower. No significant dependence is found on the metallicity of the progenitor and on $\rho_{\rm ISM}$. In all cases, the emissivity is almost entirely due to the large AC grains[1].

The amount of shock-heated dust in the ejecta can be derived from infrared observations of SN remnants. A notable (and debated) case is that of Cas A, the remnant from an historical SN which shows infrared emission from the region between the forward and reverse shocks. The identity of Cas A's progenitor is still highly debated. A star of 15-25 $M_\odot$ that loses its hydrogen envelope through winds (Chevalier 2006) or binary interactions (Young et al. 2006) and then undergoes an energetic explosion can match all the available observational constraints. In particular, the age and dynamics suggest a mass for the ejecta of 3 $M_\odot$, with about the same amount of gas reached by the reverse shock in the ejecta and swept by the forward shock in the surrounding ISM (Truelove & McKee 1999). Given these uncertainties, and the dependence of the predicted dust masses on the stellar progenitor (see Fig. 5), we can only give a tentative estimate of the amount of dust predicted for Cas A by our model. An ejecta evolution compatible with observations can be obtained for a 12 $M_\odot$ progenitor, provided we neglect the hydrogen mass. In such a model, $\approx$0.1 $M_\odot$ of dust forms. By the age of the remnant ($\sim$325 yr), $\approx$0.05 $M_\odot$ survives in the region reached by the reverse shock, where it is heated by the hot gas. We also need to consider the contribution to emission from dust in the ISM reached by the forward shock. Typically, dust in the shocked ISM is exposed to a gas of similar density and temperature to those in the reverse shock (van der Swaluw et al. 2001). For a standard value of the ISM gas-to-dust mass ratio, one would roughly expect a similar mass of emitting dust in the ISM. Thus, a model for Cas A remnant would have about 0.1 $M_\odot$ of emitting dust.

This mass appears to be more than an order of magnitude larger than what could be derived fitting the observed Spectral Energy distribution (SED) of Cas A (Hines et al. 2004). Using the emissivity predicted for SN dust, the flux in the wavelength range $10 \leqslant \lambda/\mu m \leqslant 100$ can be reasonably well reproduced with a single modified blackbody with temperature $T = 100$K, and a dust mass of 4×10^{-3} $M_\odot$ (Fig. 7, solid line). Hines et al. (2004) obtain for the cold, more massive component a similar dust mass with $T = 80$K. However, the large uncertainties and the limited FIR coverage allow to fit, equally well, a two-component model with temperatures 110 and 35K and masses, respectively, of 3×10^{-3} and 0.1 $M_\odot$ (Fig. 7, dashed line). Unfortunately Cas A lies on the line of sight of dense molecular clouds which do not allow a reliable estimate of the cold dust mass from observations at longer wavelengths in the FIR and sub-mm. Still, upper limits on the dust mass in the remnant are compatible with our model predictions (Krause et al. 2004).

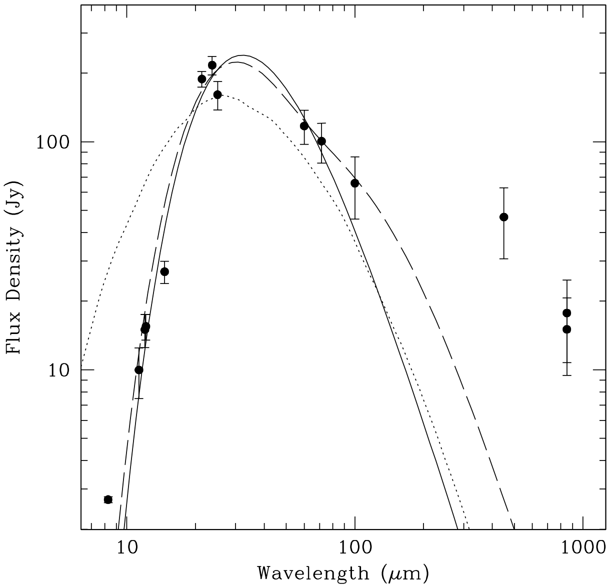

Figure 7. Synchrotron-subtracted SED of dust emission in CasA. Data points are from Hines et al. (2004). The solid line is a one-component modified blackbody fit to the data for $\lambda \leqslant 100\mu$m ($T \approx 100$K, $M_{\rm d} \approx 4.0 \times 10^{-3} M_\odot$). The dashed line is a two-component fit with $T \approx 110$K, $M_{\rm d} \approx 3.0\times10^{-3} M_\odot$ and $T \approx 35$K, $M_{\rm d} \approx 0.1 M_\odot$. The dotted line is the spectrum from stochastically heated dust in our model. See text for details.

A broad span of temperatures is clearly needed for a reliable estimate of the dust mass in the remnant. In Fig. 7 we also show the SED of the shock heated dust in the CasA model (dotted line). Because of stochastic heating (Appendix A), grains have temperatures mainly ranging from 10 to 100K. The SED cannot be easily modelled using a 2-component modified blackbody: the longer wavelength side could be described with a cold component of $T \approx 60$K, which would underestimate the dust mass by about a factor 5; instead, a hot component at $T \approx 150$K would leave a substantial residual in the fit at $\lambda \lesssim 10\mu$m. When comparing to the data for CasA, it appears that dust temperature in our models is overestimated. This could be due to an overestimate of the dust stochastic heating, to a reduction of smaller grains with respect to the dust formation model, or to differences between the emission properties of true and modelled materials. However, the uncertainties in the thermal/dynamical history of the ejecta of CasA and the impossibility of discriminating between ISM and ejecta dust emission in the spectrum prevent a more detailed analysis.

---

[1] For the same reason, increasing the minimum cluster size $\mathcal{N}$ and/or decreasing the sticking coefficient α does not affect the predicted extinction laws and emissivities, which are similar to those found for our reference model after the passage of the reverse shock.

5 SUMMARY

In the present work we have revisited the model of Todini & Ferrara (2001) for dust formation in the ejecta of core collapse SNe and followed the evolution of newly condensed grains from the time of formation to their survival through the passage of the reverse shock.

The main results can be summarized as follows:

(i) The new features introduced in the dust formation model have only a minor impact on AC grains but significantly affect other species (Si-bearing grains, Al_2O_3, and Fe_3O_4). For 12 - 40 $M_{\odot}$ stellar progenitors with $Z = Z_{\odot}$, the predicted $M_{\rm dust}$ ranges between 0.1 - 0.6 $M_{\odot}$; comparable values (within a factor 2) are found if the progenitors have $Z < Z_{\odot}$. The dominant grain species are AC and Fe_2O_3.

(ii) We identify the most critical parameters to be the minimum number of monomers, $\mathcal{N}$, which define a critical seed cluster, and the value of the sticking coefficient, α. Assuming $\mathcal{N} \geqslant 10$ (below which the application of standard nucleation theory is questionable) results in a great reduction of non-AC grains because these species nucleate when the gas in the ejecta is highly super-saturated and smaller seed clusters form. This effect is further enhanced if $\alpha < 1$: for $\alpha = 0.1$ and stellar progenitor masses $M_{\rm star} < 20 M_{\odot}$, the total mass of dust is reduced to values in the range 0.001-0.1 $M_{\odot}$, comparable to those inferred from the IR emission at 400-700 days after the explosion for 1987A and 2003gd, the only two core-collapse SNe for which these data were available.

(iii) Using a semi-analytical model to describe the dynamics of the reverse shock, we have found that thermal and non-thermal sputtering produce a shift of the size distribution function towards smaller grains; the resulting dust mass reduction depends on the density of the surrounding ISM: for $\rho_{\rm ISM} = 10^{-25}, 10^{-24}, 10^{-23}$ g cm^{-3}, about 20%, 7%, and 2% (respectively) of the initial dust mass survives. Most of dust consumption occurs within one characteristic time from the explosion, about $4 - 8 \times 10^4$ yr for core-collapse SNe. Thus, the impact of the reverse shock needs to be taken into account when comparing model predictions with observations of young SN remnants.

(iv) Averaging over a Salpeter IMF, we have derived dust extinction and emissivity. We find that the extinction curve is dominated by AC and Fe_3O_4 grains with radii larger than 20 Å. As a result, it is relatively flat in the range 1500-2500Å and then rises in the far UV. Thus, the peculiar behaviour of the extinction produced by SN dust, which has been successfully used to interpret observations of a reddened QSO at $z = 6.2$ (Maiolino et al. 2004), is preserved in the present model, and it is further amplified by the modifications induced by the passage of the reverse shock.

(v) Using dust emissivity predicted by the model, we can reproduce the observed IR flux from the young SN remnant CasA adopting a single modified black-body of temperature $T = 100$ K, which implies a mass of warm dust of $4 \times 10^{-3} M_{\odot}$, consistent with Hines et al. (2004). However, the limited observational coverage in the FIR allows to equally well reproduce the data adding a cold component with temperature $T = 35$ K and dust mass of $0.1 M_{\odot}$. According to our model, such a mass of dust is what would be produced by a single 12 $M_{\odot}$ star that has exploded after losing its hydrogen envelope, a plausible candidate for the highly debated CasA's progenitor. Because of the stochastic heating of small grains by collisions with hot gas electrons, dust in the shocked gas is predicted to have temperatures ranging from 10 to 100K.

We conclude that our study supports the idea that core-collapse SNe can be major dust factories. At the same time, it shows that our knowledge of dust condensation and its survival in SN ejecta still lacks to control some critical parameters, which prevent reliable estimates of condensation efficiencies, especially for the less massive progenitors. Within these uncertainties, the model can accomodate the still sparse observational probes of the presence of dust in SN and SN remnants.

ACKNOWLEDGMENTS

We are grateful to A. Ferrara for profitable discussions and suggestions, and to L. Del Zanna for kindly providing us the results of 1-D hydrodynamical simulations. We also acknowledge DAVID members[2] for fruitful comments and Cristiano Porciani for precious help.

REFERENCES

Beelen A., Cox P., Benford D. J., Dowell C. D., Kovács A., Bertoldi F., Omont A., Carilli C. L., 2006, ApJ, 642, 694
Begemann B., Dorschner J., Henning T., Mutschke H., Guertler J., Koempe C., Nass R., 1997, ApJ, 476, 199
Bertoldi F., Carilli C. L., Cox P., Fan X., Strauss M. A., Beelen A., Omont A., Zylka R., 2003, A&A, 406, L55
Bianchi S., Ferrara A., 2005, MNRAS, 358, 379
Chase M. W., Davies C. A., Downey J. R., Frurip D. J., McDonald R. A., Syverud A. N., 1985, J. Phys. Chem. Ref. Data, 14, Suppl. 1
Chevalier R. A., 2006, in STScI Symposium on Massive Stars From progenitor to afterlife
Clayton D. D., Deneault E. A.-N., Meyer B. S., 2001, ApJ, 562, 480
Clayton D. D., Nittler L. R., 2004, ARA&A, 42, 39
Del Zanna L., Bucciantini N., Londrillo P., 2003, A&A, 400, 397
Ditmars D. A., Ishihara S., Chang S. S., Bernstein G., West E. D., 1982, Journal of Research of the National Bureau of Standards, 87, 159
Draine B. T., 1979, Ap&SS, 65, 313
Draine B. T., Hao L., 2002, ApJ, 569, 780
Draine B. T., Li A., 2001, ApJ, 551, 807
Draine B. T., Salpeter E. E., 1979, ApJ, 231, 438
Dunne L., Eales S., Ivison R., Morgan H., Edmunds M., 2003, Nature, 424, 285
Dwek E., 1986, ApJ, 302, 363
Dwek E., 2005, in Popescu C. C., Tuffs R. J., eds, AIP Conf. Proc. 761: The Spectral Energy Distributions of Gas-Rich Galaxies: Confronting Models with Data Interstellar dust: what is it, how does it evolve, and what are its observational consequences?. pp 103–

---

[2] http://www.arcetri.astro.it/science/cosmology

Elmhamdi A., Danziger I. J., Chugai N., Pastorello A., Turatto M., Cappellaro E., Altavilla G., Benetti S., Patat F., Salvo M., 2003, MNRAS, 338, 939
Ercolano B., Barlow M. J., Sugerman B. E. K., 2007, MNRAS
Feder J., Russell K. C., Lothe J., Pound G. M., 1966, Advances in Physics, 15, 111
Freudling W., Corbin M. R., Korista K. T., 2003, ApJL, 587, L67
Gail H.-P., 2003, in Henning T. K., ed., LNP Vol. 609: Astromineralogy Formation and Evolution of Minerals in Accretion Disks and Stellar Outflows. pp 55–120
Gail H.-P., Keller R., Sedlmayr E., 1984, A&A, 133, 320
Green D. A., Tuffs R. J., Popescu C. C., 2004, MNRAS, 355, 1315
Guhathakurta P., Draine B. T., 1989, ApJ, 345, 230
Henning T., Mutschke H., 1997, A&A, 327, 743
Hines D. C., Krause O., Rieke G. H., Fan X., Blaylock M., Neugebauer G., 2006, ApJL, 641, L85
Hines D. C., Rieke G. H., Gordon K. D., Rho J., Misselt K. A., Woodward C. E., Werner M. W., Krause O., Latter W. B., Engelbracht C. W., Egami E., Kelly D. M., Muzerolle J., Stansberry J. A., Su K. Y. L., Morrison J. E., Young E. T., Noriega-Crespo A., et al. 2004, ApJS, 154, 290
Hirashita H., Nozawa T., Kozasa T., Ishii T. T., Takeuchi T. T., 2005, MNRAS, 357, 1077
Hopkins P. F., Strauss M. A., Hall P. B., Richards G. T., Cooper A. S., Schneider D. P., Vanden Berk D. E., Jester S., Brinkmann J., Szokoly G. P., 2004, AJ, 128, 1112
Jäger C., Dorschner J., Mutschke H., Posch T., Henning T., 2003, A&A, 408, 193
Jones A. P., Tielens A. G. G. M., Hollenbach D. J., McKee C. F., 1994, ApJ, 433, 797
Kelley K. K., 1943, Journal of the American Chemical Society, 65, 339
Koenitzer J. W., Keesom P. H., Honig J. M., 1989, Phys. Rev. B, 39, 6231
Koike C., Kaito C., Yamamoto T., Shibai H., Kimura S., Suto H., 1995, Icarus, 114, 203
Kozasa T., Hasegawa H., 1987, Progress of Theoretical Physics, 77, 1402
Kozasa T., Hasegawa H., Nomoto K., 1991, A&A, 249, 474
Krause O., Birkmann S. M., Rieke G. H., Lemke D., Klaas U., Hines D. C., Gordon K. D., 2004, Nature, 432, 596
Krupka K. M., Robie R. A., Hemingway B. S., Kerrik D. M., Ito J., 1985, American Mineralogist, 70, 249
Leger A., Jura M., Omont A., 1985, A&A, 144, 147
Leitch-Devlin M. A., Williams D. A., 1985, MNRAS, 213, 295
Maiolino R., Juarez Y., Mujica R., Nagar N. M., Oliva E., 2003, ApJL, 596, L155
Maiolino R., Schneider R., Oliva E., Bianchi S., Ferrara A., Mannucci F., Pedani M., Roca Sogorb M., 2004, Nature, 431, 533
Marchenko S. V., 2006, in Lamers H. J. G. L. M., Langer N., Nugis T., Annuk K., eds, ASP Conf. Ser. 353: Stellar Evolution at Low Metallicity: Mass Loss, Explosions, Cosmology Dust Production in the High-Redshift Universe. pp 299–
Mie G., 1908, Ann. Phys., 25, 377
Morgan H. L., Edmunds M. G., 2003, MNRAS, 343, 427
Mukai T., 1989, in Bonetti A., Greenberg J. M., Aiello S., eds, Evolution of Interstellar Dust and Related Topics Cometary Dust and Interplanetary Particles. pp 397–
Nozawa T., Kozasa T., Habe A., 2006, ApJ, 648, 435
Nozawa T., Kozasa T., Umeda H., Maeda K., Nomoto K., 2003, ApJ, 598, 785
Pei Y. C., 1992, ApJ, 395, 130
Pentericci L., Fan X., Rix H.-W., Strauss M. A., Narayanan V. K., Richards G. T., Schneider D. P., Krolik J., Heckman T., Brinkmann J., Lamb D. Q., Szokoly G. P., 2002, AJ, 123, 2151
Philipp H. R., 1985, in Palik E. D., ed., , Handbook of Optical Constants of Solid. Academic Press, New York, p. 719
Robson I., Priddey R. S., Isaak K. G., McMahon R. G., 2004, MNRAS, 351, L29
Schneider R., Ferrara A., Salvaterra R., 2004, MNRAS, 351, 1379
Shepherd J. P., Koenitzer J. W., Aragón R., Sandberg C. J., Honig J. M., 1985, Phys. Rev. B, 31, 1107
Sugerman B. E. K., Ercolano B., Barlow M. J., Tielens A. G. G. M., Clayton G. C., Zijlstra A. A., Meixner M., Speck A., Gledhill T. M., Panagia N., Cohen M., Gordon K. D., Meyer M., Fabbri J., Bowey J. E., Welch D. L., Regan M. W., Kennicutt R. C., 2006, Science, 313, 196
Todini P., Ferrara A., 2001, MNRAS, 325, 726
Truelove J. K., McKee C. F., 1999, ApJS, 120, 299
van der Swaluw E., Achterberg A., Gallant Y. A., Tóth G., 2001, A&A, 380, 309
Wooden D. H., Rank D. M., Bregman J. D., Witteborn F. C., Tielens A. G. G. M., Cohen M., Pinto P. A., Axelrod T. S., 1993, ApJS, 88, 477
Woosley S. E., Weaver T. A., 1995, ApJS, 101, 181
Young P. A., Fryer C. L., Hungerford A., Arnett D., Rockefeller G., Timmes F. X., Voit B., Meakin C., Eriksen K. A., 2006, ApJ, 640, 891
Zubko V. G., Mennella V., Colangeli L., Bussoletti E., 1996, MNRAS, 282, 1321

APPENDIX A: STOCHASTIC HEATING FROM ELECTRON COLLISIONS

We have derived the temperature distribution $P(T_\mathrm{d})$ following the method of Guhathakurta & Draine (1989), to which we refer for a more detailed description.

We have divided the range of possible dust temperatures into N_b bins. For the case studied here, we found sufficient to define $N_\mathrm{b} = 500$ bins, logarithmically spaced in the range $2 < T_\mathrm{d}/\mathrm{K} < 2000$. The i-bin has temperature $T_{\mathrm{d},i}$, energy E_i and energy width ΔE_i. The energy corresponding to each value of T_d is defined as

$$E(T_\mathrm{d}) = \int_0^{T_\mathrm{d}} C(T) dT,$$

where C is the specific heat, which is derived by fitting experimental data. We have adopted a piecewise power-law of the form

$$C(T) = A\, T^B.$$

The fitted values for A and B are given in Table A1.

Table A1. Thermal and optical properties of SNe dust materials

Materials	A (erg cm^3 K^{-1})	B	Specific heat range in T (K)	Refs.	Refractive index Refs.
Al_2O_3	4.44	3	$(0, 110]$	Ditmars et al. (1982)	Koike et al. (1995, *ISAS)*
	1.22 10^2	2.29	$(110, 200]$	Chase et al. (1985)	Begemann et al. (1997, *compact)*
	7.00 10^5	0.66	$(200, 500]$		
	1.45 10^7	0.17	$(500, 2000]$		
	5.44 10^7	0	$(2000, \infty)$		
Fe_3O_4	22.5	3	$(0, 10]$	Chase et al. (1985)	Mukai (1989)
	7.65	3.47	$(10, 30]$	Shepherd et al. (1985)	
	3.74 10^2	2.32	$(30, 80]$	Koenitzer et al. (1989)	
	1.04 10^5	1.04	$(80, 300]$		
	3.95 10^7	0	$(300, \infty)$		
$MgSiO_3$	9.22	3	$(0, 20]$	Kelley (1943)	Jäger et al. (2003)
	2.01	3.51	$(20, 50]$	Chase et al. (1985)	
	7.94 10^2	1.98	$(50, 130]$	Krupka et al. (1985)	
	1.32 10^5	0.93	$(130, 400]$		
	3.47 10^7	0	$(400, \infty)$		
Mg_2SiO_4	22.7	3	$(0, 60]$	Kelley (1943)	Jäger et al. (2003)
	6.45 10^2	2.18	$(60, 120]$	Chase et al. (1985)	
	1.40 10^5	1.06	$(120, 300]$		
	1.42 10^7	0.25	$(300, 2000]$		
	9.44 10^7	0	$(2000, \infty)$		
AC	3.82 10^2	2	$(0, 70]$	Chase et al. (1985)	Zubko et al. (1996, *ACAR)*
	3.27 10^3	1.50	$(70, 300]$	Draine & Li (2001)	
	5.58 10^4	1.00	$(300, 700]$		
	1.09 10^7	0.19	$(700, 3000]$		
	5.09 10^7	0	$(3000, \infty)$		
SiO_2	9.95 10^2	2	$(0, 60]$	Chase et al. (1985)	Philipp (1985)
	5.50 10^4	1.02	$(60, 500]$	Leger et al. (1985)	Henning & Mutschke (1997)
	3.11 10^7	0	$(500, \infty)$		

The function $P(T_{\rm d})$ is computed from the transition matrix between the initial and final internal energy states, $A_{f,i}$. The probability per unit time that a dust grain in the energy state E_i is heated to the energy state E_f (with $f > i$) by collisions with electrons is given by

$$A_{f,i} = \begin{cases} n\ \pi a^2 \Delta E_f \times & \\ \left[\sqrt{\dfrac{2(E_f - E_i)}{m}} f(E_f - E_i) + \right. & \text{if } E_f - E_i < E_\star \\ \left. \sqrt{\dfrac{2E_{\rm eff}}{m}} f(E_{\rm eff}) \dfrac{\sqrt{1-(E_f-E_i)/E_{\rm eff}}}{1-\sqrt{1-(E_f-E_i)/E_{\rm eff}}} \right], & \\ 0 & \text{otherwise.} \end{cases}$$

In the above equation, n and m are the electron number density and mass, respectively, and $f(E)$ is the Maxwell distribution function defined such that $nf(E)\Delta E$ is the number of electrons of energy E per unit volume. $E_\star$ is the maximum energy that an electron can transfer to a dust grain (Dwek 1986). If $E_f - E_i > E_\star$ it is not possible to jump from stage i to stage f through electron collisions; if $E_f - E_i < E_\star$ the jump is allowed for all electrons with energy $E_f - E_i$ (which will transfer their entire energy to the grain) and for the electrons with energy $E_{\rm eff}$ (which will transfer an energy $E_{\rm eff}\zeta(E_{\rm eff}) = E_f - E_i$; the function $\zeta(E)$ is the fraction of the electron energy which is deposited on a dust grain when $E > E_\star$, as defined in Dwek 1986).

As in Guhathakurta & Draine (1989) only cooling terms from level f+1 to level f are considered:

$$A_{f,f+1} = \frac{4\pi}{E_{f+1} - E_f} \int_0^\infty \pi a^2 Q_{\rm abs}(a,\lambda)\ B_\lambda(T_{{\rm d},f+1}) d\lambda,$$

where B_λ is the Planck function and $Q_{\rm abs}(a,\lambda)$ the absorption efficiency of a grain of radius a. Values for $Q_{\rm abs}(a,\lambda)$ were derived using the Mie's (1908) theory for spherical dust grains, adopting the refractive index from the references in Table A1.

In Fig. A1 we show the temperature distributions for AC and Fe_3O_4 dust grains of radii a=10, 50 and 200Å. Grains are exposed to a gas with $T = 10^8$K and $n = 10$ electrons cm^{-3}, typical conditions encountered in the ejecta swept by the reverse shock. Smaller grains have broader temperature distributions, with a high temperature tail.

Using the sublimation rate of Draine & Hao (2002), we have derived a *sublimation temperature* $T_{\rm s}$, defined as the temperature necessary to completely consume a grain in about 20 yr, the typical time step of our simulation. For the grain sizes encountered in our work, we have $T_{\rm d} \gtrsim 1200$K. At

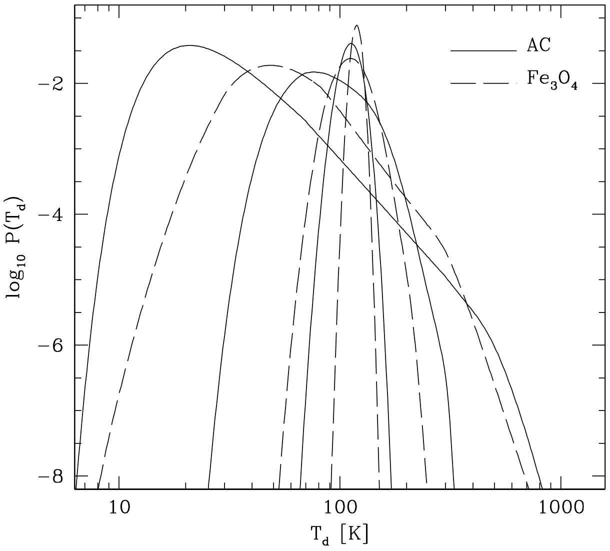

Figure A1. Temperature distributions $P(T_\mathrm{d})$ for AC and Fe_3O_4 dust grains in a hot gas with $T = 10^8$K and $n = 10$ electrons cm^{-3}. $P(T_\mathrm{d})$ is shown for radii $a = 10$ Å (broader distributions), 50 Å and 200 Å (distributions spanning a smaller range of T_d).

any time in the ejecta evolution, only a negligible fraction of all grains would exceed that temperature. As a result, dust sublimation is insignificant in our models.